Electron transport through one-dimensional lateral surface superlattices in magnetic fields

Hongqi Xu
Department of Solid State Physics, University of Lund, Box 118, S-221 00 Lund, Sweden
(Received 17 March 1995)

A scattering-matrix method for the calculations of electron transport through lateral quantum systems in the presence of a perpendicular magnetic field is developed and is used to investigate the effects of an applied magnetic field on electron transport through a quantum channel modulated by a smooth periodic potential along the direction of the current flow. At zero magnetic field, the calculated conductance displays regular dips due to the formation of minigaps (or the Bragg reflections) and the rapid oscillations due to electron transmission through the coupled quasi-zero-dimensional states in the cavity regions between the potential barriers. Both are shown to be suppressed when a magnetic field is applied to the quantum channel. This is interpreted as the formation of propagating edge states. However, other irregular dips are shown to appear in the conductance of the modulated channel in the presence of the magnetic field. These dips reflect the coupling between the electron states propagating along the opposite edges of the channel and may appear so densely in a wide quantum channel with a strong modulation that the conductance exhibits fluctuations. In the high-field regime where the magnetic length l_B is much smaller than the channel width w, these irregular dips are seen to be also suppressed, leading to a nearly perfect recovery of the conductance quantization.

I. INTRODUCTION

Recent advances in submicrometer technology have made it possible to confine the electrons of a two-dimensional electron gas (2DEG) in a semiconductor heterostructure to regions with lateral dimensions on the order of 100 nm, and have naturally led to rapid development in the field of electron transport in low-dimensional systems, such as narrow quantum wires, constrictions, and quantum dots.[1–3] In such a tiny structure, the electron transport can be ballistic and the motion of electrons is governed by quantum mechanics rather than classical mechanics, revealing a few additional and interesting transport phenomena. A notable example is that in the linear-response regime, the conductance of a quasi-one-dimensional (Q1D) channel was found to be quantized in units of $2e^2/h$ at low temperatures,[4,5] while in the nonlinear-response regime, the quantization of the conductance in units of e^2/h was observed.[6,7] These fascinating phenomena have now been well understood, thanks to a number of theoretical calculations including those using adiabatic approximation and those based on exact quantum-mechanical calculations.[8–16]

If the Q1D channel is further modulated by a periodic potential or patterned with a periodic structure, minigaps of zero density of states and minibands are expected to form.[3] These lateral superlattice effects may be studied in the linear-response regime of small applied voltage by varying the Fermi energy E_F or the width of the Q1D channels. The conductance dips or wells are expected to be observed if E_F is in a minigap. In addition, for a periodically modulated channel with a finite number of unit cells, a miniband is represented by a group of discrete states. The discrete states give rise to closely spaced resonances in the transmission probability through the superlattice as a function of energy, and may thus be observed as a series of peaks in the conductance as a function of the Fermi energy or the width of the channel. A successful experiment of this type was reported by Kouwenhoven *et al.*[17]

With use of transfer-matrix methods, a number of quantum-mechanical calculations[18–23] have been made for electron transport through one-dimensional (1D) lateral superlattices. Both the grouped miniband-associated conductance peaks and the conductance dips, due to the occurrence of minigaps, were obtained. However, the applications of the methods have been very much limited by numerical instability of the methods. One may remove this numerical difficulty from the calculations by reformulating the problem with the use of the recursive Green's-function technique.[24] However, a large computing effort is often in demand in the implementation of the technique. The applications of the technique have, therefore, been primarily confined to simple quantum systems. The effects of the formation of minigaps and minibands on electron transport through 1D lateral superlattices were also studied by Leng and Lent very recently using the finite-element method.[25] In their study, the results of the transfer-matrix calculations of Refs. 18–23 were reproduced, and a one-to-one correspondence between the index of quantized conductance plateaus and the number of Bloch bands with positive group velocity was demonstrated by a comparison between the calculated conductance and the band structure. The study shows also that the one-to-one correspondence persists in the presence of an applied magnetic field. The magnetic field was disregarded in the transfer-matrix calculations of Refs. 18–23.

In this paper, we present an alternative formalism for treating the transport properties of lateral superlattices in magnetic fields, based on the scattering matrices. Previously, the scattering-matrix method was successfully

used, without suffering numerical instability, for the study of electron transport in lateral antidot lattices when no magnetic field is applied.[26] Here, we will reformulate the method to allow the presence of a magnetic field. We then report on the results of its application to a periodically modulated Q1D channel. The modulation potential will be modeled by a smooth function realistic to experimental situations. In the application, we are particularly concerned about the effects of the magnetic field on the minibands and minigaps formed in the system. We will explore them by computing the conductance of the system at a fixed magnetic field as a function of the channel width w and a function of the Fermi energy E_F.

II. SCATTERING-MATRIX TECHNIQUE IN MAGNETIC FIELDS

A scattering-matrix method has been described in details in Ref. 26 for electron transport through lateral superlattices at the zero magnetic field ($B=0$ T). Although it is elementary to reformulate the method for the cases when a magnetic field is applied, we prefer to present the reformulation for completeness, and because we need it to discuss some fundamental and computational features that appear due to the presence of the magnetic field.

Let us consider a lateral, ballistic quantum channel of finite width w, defined in the plane of a 2DEG (the x-y plane) and modulated by a periodic potential $V(x,y)$. We wish to confine ourselves to the mesoscopic regime by assuming that the quantum channel has a finite length $L_T=x_0^R-x_0^L$ and is sandwiched between two perfect semi-infinitely long leads of the same width w at equal Fermi energy E_F [see Fig. 1(a)]. The Schrödinger equation of motion of an electron with energy ε in a uniform magnetic field $\mathbf{B}=(0,0,B)$ can then be written as

$$\left[\frac{(\mathbf{P}+e\,\mathbf{A})^2}{2m^*}+V_c(y)+V(x,y)\right]\Psi(x,y)=\varepsilon\Psi(x,y)\ , \qquad (1)$$

where m^* is the effective mass, $V_c(y)$ represents the confining potential of the quantum channel in the direction perpendicular to the current flow, and $\mathbf{A}$ is the vector potential. In this work, we choose the Landau gauge, $\mathbf{A}=(-By,0,0)$, and consider only 1D modulations along the channel,

$$V(x,y)=\begin{cases} V_b(x)\ , & x_0^L\le x\le x_0^R \text{ and } -w/2\le y\le w/2 \\ 0 \text{ otherwise}\ , \end{cases} \qquad (2)$$

where $V_b(x)=V_b(x+a)$ and a is the modulation period, as schematically shown in Fig. 1(a). We further assume that $V_b(x)$ in a barrier region is in general a smooth function of x along the direction of the current flow [see Fig. 1(b), for an example].

For $V_b(x)=0$, Eq. (1) can be solved by separation of variables. However, such a separation of variables may not be achieved for a general modulation potential of the type as shown in Fig. 1, and Eq. (1) may have to be solved numerically. In this work, we prefer to solve Eq. (1) using scattering-matrix technique.

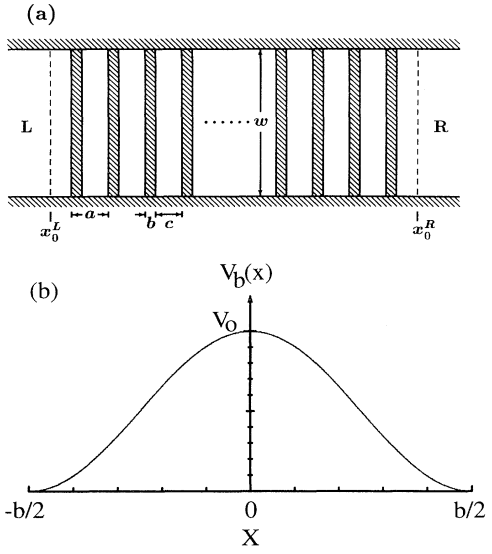

FIG. 1. Schematic view of the Q1D channel modulated periodically by a finite number M of smooth potential barriers. (a) Layout of the lateral surface superlattice. The modulated channel has a width w and is connected at x_0^L and x_0^R with two perfect leads of the same width w at equal Fermi energy E_F. When a potential difference is applied, electrons are assumed to flow from L to R, i.e., in the x direction. (b) Assumed potential profile of the barriers, $V_b(x)=V_0\cos^{2\beta}(\pi x/b)$, $[-b/2,\ b/2]$, with $\beta=1$. V_0 and β control the strength and the steepness of the modulation, respectively.

We begin with the assumption that the potential-modulated Q1D channel can be decomposed into N transverse strips and the potential in strip i can be approximated by a constant $V_b(x^i)$, where $i=1,2,\ldots,N$ and x^i may be chosen to be the x coordinate at the center of the strip.[27] Thus, Eq. (1) may be solved for strip i by separation of variables of the form

$$\psi^i(x,y)=e^{ik^ix}\varphi^i(y)\ , \qquad (3)$$

where $\varphi^i(y)$ satisfies the reduced one-dimensional Schrödinger equation,

$$\left\{-\frac{\hbar^2}{2m^*}\frac{d^2}{dy^2}+\frac{m^*}{2}\omega_c^2(y-l_B^2k^i)^2+V_c(y)+V_b(x^i)\right\}\varphi^i(y) =\varepsilon\varphi^i(y)\ . \qquad (4)$$

Here, $\omega_c\equiv eB/m^*$ is the cyclotron frequency and $l_B\equiv(\hbar/eB)^{1/2}$ the magnetic length. For electron-transport calculations, Eq. (4) is solved at a given electron energy ε for eigenwave numbers k_α^i and eigenwave functions $\varphi_\alpha^i(y)$. The properties of the functions $\varphi_\alpha^i(y)$, including the orthogonality relation and normalization, have been discussed by many authors.[28,29] For reasons to be seen later, here we choose to normalize our functions $\varphi_\alpha^i(y)$, so that

$$\langle\varphi_\alpha^i(y)|\varphi_\alpha^i(y)\rangle=1\ , \qquad (5)$$

and to define a velocity matrix $\mathbf{v}^i\equiv\{v_{\alpha\beta}^i\}$ by

$$v^i_{\alpha\beta}=\frac{\hbar}{2m^*}\int\varphi^i_\alpha(y)\left[k^i_\alpha+k^i_\beta-\frac{2y}{l_B^2}\right]\varphi^i_\beta(y)dy=v^i_\alpha\delta_{\alpha\beta}\ , \tag{6}$$

where v^i_α is a short notation for $v^i_{\alpha\alpha}$ and is known as the quantum mean velocity when it is real.

Equation (4) may be solved by using a complete basis of $\{\Phi_n(y)\}$ satisfying

$$\left[-\frac{\hbar^2}{2m^*}\frac{d^2}{dy^2}+V_c(y)\right]\Phi_n(y)=\varepsilon_n\Phi_n(y)\ . \tag{7}$$

In this basis, the wave function $\varphi^i_\alpha(y)$ is written as

$$\varphi^i_\alpha(y)=\sum_n d^i_{n\alpha}\Phi_n(y)\ , \tag{8}$$

while Eq. (4) as

$$\sum_n\left\{\frac{1}{\varepsilon_w}[\varepsilon-\varepsilon_n-V_b(x^i)]\delta_{mn}-\left[\frac{\hbar\omega_c}{2\varepsilon_w}\right]^2Y^2_{mn}+\left[\frac{\hbar\omega_c}{\varepsilon_w}\right]\left[\frac{k^i_\alpha w}{\pi}\right]Y_{mn}-\left[\frac{k^i_\alpha w}{\pi}\right]^2\delta_{mn}\right\}d^i_{n\alpha}=0\ , \tag{9}$$

where

$$Y^2_{mn}=\left[\frac{\pi}{w}\right]^2\langle\Phi_m(y)|y^2|\Phi_n(y)\rangle\ , \tag{10}$$

$$Y_{mn}=\left[\frac{\pi}{w}\right]\langle\Phi_m(y)|y|\Phi_n(y)\rangle\ , \tag{11}$$

and $\varepsilon_w=(\hbar^2/2m^*)(\pi/w)^2$.

Equation (9) is solved in an expanded basis, due to Tamura and Ando[30] as follows. By introducing auxiliary coefficients $f^i_{n\alpha}=(k^i_\alpha w/\pi)d^i_{n\alpha}$, we can rewrite Eq. (9) as

$$\begin{bmatrix}\mathbf{0} & \mathbf{1}\\ \mathbf{S} & \mathbf{T}\end{bmatrix}\begin{bmatrix}\mathbf{d}^i\\ \mathbf{f}_i\end{bmatrix}=k^i_\alpha\begin{bmatrix}w/\pi & \\ & \end{bmatrix}\begin{bmatrix}\mathbf{d}^i\\ \mathbf{f}^i\end{bmatrix}\ , \tag{12}$$

with

$$(\mathbf{S})_{mn}=\frac{1}{\varepsilon_w}[\varepsilon-\varepsilon_n-V_b(x^i)]\delta_{mn}-\left[\frac{\hbar\omega_c}{2\varepsilon_w}\right]^2Y^2_{mn}\ , \tag{13}$$

$$(\mathbf{T})_{mn}=\left[\frac{\hbar\omega_c}{\varepsilon_w}\right]Y_{mn}\ . \tag{14}$$

Solving Eq. (12) for a given energy ε, we obtain a set of eigenwave numbers $\{k^i_\alpha\}$ and a set of corresponding eigenwave functions $\{\varphi^i_\alpha(y)\}$. Inserting them into Eq. (3), eigensolutions $\{\psi^i_\alpha(x,y)\}$ in the strip region i are then obtained.

The transport property of these eigensolutions is determined by their wave numbers $\{k^i_\alpha\}$. These wave numbers can be real, imaginary, or complex. Only those eigensolutions whose wave numbers are real represent propagating modes, while the others correspond to evanescent or exploding modes. In order to overcome the difficulty in numerical calculations due to the presence of the exploding modes, we shall divide our eigensolutions into two groups and adopt the scattering-matrix formalism. The first group, in which the eigenwave functions are denoted by $\{k^i_{I\alpha}\}$ and $\{\varphi^i_{I\alpha}(y)\}$, consists of those modes whose wave number has a positive imaginary part and those modes whose wave number has a null imaginary part, but a positive real part, while the second group, in which the eigenwave numbers and eigenwave functions are denoted by $\{k^i_{II\alpha}\}$ and $\{\varphi^i_{II\alpha}(y)\}$, consists of all the rest, i.e., those modes whose wave number has a negative imaginary part and those modes whose wave number has a null imaginary part, but a negative real part. In fact, the eigensolutions in the first group, denoted by $\{\psi^i_{I\alpha}(x,y)\}$, are those modes that are propagating forwards or evanescent, while the eigensolutions in the second group, denoted by $\{\psi^i_{II\alpha}(x,y)\}$, are those that are propagating backwards or exploding.

In terms of these notations, the wave function $\Psi^i(x,y)$ of an electron with energy ε in strip region i can then be written as

$$\begin{aligned}\Psi^i(x,y)&=\sum_\alpha[a^i_{I\alpha}e^{ik^i_{I\alpha}(x-x^i_0)}\varphi^i_{I\alpha}(y)+a^i_{II\alpha}e^{ik^i_{II\alpha}(x-x^i_0)}\varphi^i_{II\alpha}(y)]\\&=\sum_{n\alpha}\Phi_n(y)[d^i_{In\alpha}a^i_{I\alpha}e^{ik^i_{I\alpha}(x-x^i_0)}+d^i_{IIn\alpha}a^i_{II\alpha}e^{ik^i_{II\alpha}(x-x^i_0)}]\ ,\end{aligned} \tag{15}$$

where x^i_0 is the reference coordinate along the x direction for the strip region i. The calculation for electron transport should not depend on the choice of x^i_0. Thus, for simplicity, we chose a set of $\{x^i_0\}$, such that $x^1_0=x^L_0$, $x^{N+1}_0=x^R_0$, and $x^{i+1}_0-x^i_0=l^i$, where l^i is the width of the ith narrow strip. Furthermore, since the velocity matrix $\mathbf{v}^i$ is diagonal, it can immediately be written as

$$\mathbf{v}^i=\mathbf{v}^i_I\oplus\mathbf{v}^i_{II}\ , \tag{16}$$

with $\mathbf{v}^i_I=\{v^i_{I\alpha}\}$ and $\mathbf{v}^i_{II}=\{v^i_{II\alpha}\}$, where $v^i_{I\alpha}(v^i_{II\alpha})$ is the velocity matrix element calculated from Eq. (6) with the eigenwave number $k^i_{I\alpha}(k^i_{II\alpha})$ and the eigenwave function $\varphi^i_{I\alpha}(\varphi^i_{II\alpha})$ in the first (second) group.

Obviously, we have a set of unknown coefficients $\{a^i_{I\alpha}\}$ and $\{a^i_{II\alpha}\}$ in the expansion of the wave function $\Psi^i(x,y)$ in each transverse strip region. However, the connection between the expansion coefficients $\{a^i_{I\alpha}\}$ and $\{a^i_{II\alpha}\}$ in the strip region i and the expansion coefficients $\{a^{i+1}_{I\alpha}\}$ and $\{a^{i+1}_{II\alpha}\}$ in strip region $i+1$ can be achieved via a transfer matrix $\mathbf{M}(i,i+1)$,

$$\begin{bmatrix}\mathbf{A}^i_I\\ \mathbf{A}^i_{II}\end{bmatrix}=\mathbf{M}(i,i+1)\begin{bmatrix}\mathbf{A}^{i+1}_I\\ \mathbf{A}^{i+1}_{II}\end{bmatrix}\ , \tag{17}$$

where $\mathbf{A}^i_I$ and $\mathbf{A}^i_{II}$ are coefficient vectors containing $\{a^i_{I\alpha}\}$ and $\{a^i_{II\alpha}\}$, respectively. It is elementary to show that the transfer matrix $\mathbf{M}(i,i+1)$ can be written as

$$\mathbf{M}(i,i+1)=\begin{bmatrix}\gamma^i_I & \mathbf{0}\\ \mathbf{0} & \gamma^i_{II}\end{bmatrix}^{-1}\begin{bmatrix}\mathbf{v}^i_I & \mathbf{0}\\ \mathbf{0} & \mathbf{v}^i_{II}\end{bmatrix}^{-1}\mathbf{T}(i,i+1)\ , \tag{18}$$

where γ_I^i and γ_{II}^i are two diagonal matrices with elements given by

$$(\gamma_I^i)_{\alpha\alpha}=\exp(ik_{I\alpha}^i l^i) ,$$
$$(\gamma_{II}^i)_{\alpha\alpha}=\exp(ik_{II\alpha}^i l^i) , \tag{19}$$

and $\mathbf{T}(i,i+1)$ is the matrix defined by

$$\mathbf{T}(i,i+1)=\frac{1}{2}\begin{bmatrix}\tilde{\mathbf{Q}}_I^i & \tilde{\mathbf{P}}_I^i\\ \tilde{\mathbf{Q}}_{II}^i & \tilde{\mathbf{P}}_{II}^i\end{bmatrix}\begin{bmatrix}\mathbf{P}_I^{i+1} & \mathbf{P}_{II}^{i+1}\\ \mathbf{Q}_I^{i+1} & \mathbf{Q}_{II}^{i+1}\end{bmatrix} , \tag{20}$$

with the submatrices $\mathbf{P}_{I,II}^i$ and $\mathbf{Q}_{I,II}^i$ given by

$$(\mathbf{P}_I^i)_{n\alpha}=d_{In\alpha}^i ,$$
$$(\mathbf{P}_{II}^i)_{n\alpha}=d_{IIn\alpha}^i , \tag{21}$$

$$(\mathbf{Q}_I^i)_{n\alpha}=\sum_m d_{Im\alpha}^i\left[\frac{\hbar k_{I\alpha}^i}{m^*}\delta_{nm}-w_c Y_{nm}\right] ,$$
$$(\mathbf{Q}_{II}^i)_{n\alpha}=\sum_m d_{IIm\alpha}^i\left[\frac{\hbar k_{II\alpha}^i}{m^*}\delta_{nm}-w_c Y_{nm}\right] . \tag{22}$$

The *tilde* "~" in Eq. (20) denotes the matrix transpose. Here, we note that although the matrices $\mathbf{P}_I^i$ and $\mathbf{P}_{II}^i$ are seen to remain in the same form as we derived in Ref. 26, the matrices $\mathbf{Q}_I^i$ and $\mathbf{Q}_{II}^i$ are found to differ from that in Ref. 26. The fundamental difference is the appearance of the term $w_c Y_{nm}$ in the brackets of Eq. (22), due to the presence of the magnetic field. The connection between the expansion coefficients of the electron wave function in the two perfect leads may be written as

$$\begin{bmatrix}\mathbf{A}_I^L\\ \mathbf{A}_{II}^L\end{bmatrix}=\mathbf{M}(L,R)\begin{bmatrix}\mathbf{A}_I^R\\ \mathbf{A}_{II}^R\end{bmatrix} , \tag{23}$$

where $\mathbf{A}_I^L$ and $\mathbf{A}_{II}^L$ are the coefficient vectors containing $\{a_{I\alpha}^L\}$ and $\{a_{II\alpha}^L\}$, $\mathbf{A}_I^R$ and $\mathbf{A}_{II}^R$ are the coefficient vectors containing $\{a_{I\alpha}^R\}$ and $\{a_{II\alpha}^R\}$, and $\mathbf{M}(L,R)$ is the total transfer matrix of the system given by

$$\mathbf{M}(L,R)=\mathbf{M}(L,1)\times\prod_{i=1}^{N-1}\mathbf{M}(i,i+1)\times\mathbf{M}(N,R) . \tag{24}$$

Here, $\mathbf{M}(L,1)$ and $\mathbf{M}(N,R)$ are the two transfer matrices that couple the wave function in the quantum constriction to the wave function in the two perfect leads.

It is well known that in the calculations for the total transfer matrix $\mathbf{M}(L,R)$, one often suffers a numerical instability due to the presence of both exponentially growing and exponentially decaying terms in the formulation.[26,31] This problem may be removed by rewriting Eq. (23) as

$$\begin{bmatrix}\mathbf{A}_I^R\\ \mathbf{A}_{II}^L\end{bmatrix}=\mathbf{S}(L,R)\begin{bmatrix}\mathbf{A}_I^L\\ \mathbf{A}_{II}^R\end{bmatrix} , \tag{25}$$

where $\mathbf{S}(L,R)$ is known as the scattering matrix of the system and can be obtained iteratively with the help of the transfer matrix $\mathbf{M}(i,i+1)$. For details of this procedure, we refer to our earlier work of Ref. 26.

A unique solution of the Schrödinger equation of the quantum system can only be obtained after we impose a boundary condition on the electron wave function. Here, we are interested in such electron states that may carry the electric current through the quantum system. Thus, let us consider an electron of energy ε in the left lead in a state, $E^{ik_{I\gamma}^L(x-x_0^L)}\varphi_{I\gamma}^L(y)$, propagating forward from left to right. After being scattered in the potential-modulated channel, the wave function of the electron in the left and right leads should be written as

$$\Psi^L(x,y)=e^{ik_{I\gamma}^L(x-x_0^L)}\varphi_{I\gamma}^L(y)+\sum_\alpha a_{II\alpha}^L e^{ik_{II\alpha}^L(x-x_0^L)}\varphi_{II\alpha}^L(y) , \tag{26}$$

$$\Psi^R(x,y)=\sum_\alpha a_{I\alpha}^R e^{ik_{I\alpha}^R(x-x_0^R)}\varphi_{I\alpha}^R(y) . \tag{27}$$

Thus, the boundary condition imposed on the wave function of the electron is

$$\begin{bmatrix}\mathbf{A}_I^L\\ \mathbf{A}_{II}^R\end{bmatrix}=\begin{bmatrix}\mathbf{I}_\gamma\\ \mathbf{0}\end{bmatrix} , \tag{28}$$

where $\mathbf{I}_\gamma$ is a unit vector with elements given by $(\mathbf{I}_\gamma)_\alpha=\delta_{\alpha\gamma}$. The wave-function coefficients $\mathbf{A}_I^R$ and $\mathbf{A}_{II}^L$ are simply obtained by inserting this boundary condition into Eq. (25).

At $T=0$, the conductance of the quantum constriction in the linear-response regime can be written as

$$G=-\frac{e}{\pi\hbar}\sum_\gamma^{(R)}J(E_F,k_{I\gamma}^L)/v_{I\gamma}^L , \tag{29}$$

where $J(E_F,k_{I\gamma})$ is the current carried through the quantum system by the electron state associated with the incident wave $e^{ik_{I\gamma}^L(x-x_0^L)}\varphi_{I\gamma}^L(y)$ at energy E_F [see Appendix for a derivation of the current $J(E_F,k_{I\gamma})$], and (R) indicates that the sum is taken over those values of γ for which $k_{I\gamma}^L$ and thus $v_{I\gamma}^L$ [see Eq. (6)] are real. In terms of the expansion coefficients of the wave function in the perfect leads, the conductance is simply given by

$$G=\frac{2e^2}{h}\sum_\gamma^{(R)}\left[1+\sum_\alpha^{(R)}\frac{v_{II\alpha}^L}{v_{I\gamma}^L}|a_{II\alpha}^L|^2\right]=\frac{2e^2}{h}\sum_\gamma^{(R)}\sum_\alpha^{(R)}\frac{v_{I\alpha}^R}{v_{I\gamma}^L}|a_{I\alpha}^R|^2 . \tag{30}$$

Compared with what we obtained in Ref. 26 at the zero magnetic field, the quantum mean velocity (instead of the wave vector) is seen to enter the expressions of the conductance, Eqs. (29) and (30). Note that Eq. (30) is the multichannel Landauer-Büttiker formula in a magnetic field and has been derived in many different ways.[32–34]

The method presented in this section is formulated in a basis of infinite order and is exact. However, Eq. (9) or (12) has to be solved numerically by truncating m and n at a high transverse level K. In the actual calculations, we set K as large as it is necessary to obtain a desired convergence in the conductance.

III. PERIODICALLY MODULATED QUASI-ONE-DIMENSIONAL CHANNEL IN MAGNETIC FIELDS

We will now apply our theoretical formulation to study the magnetoconductance of a Q1D channel modulated by a periodic potential containing a finite number M of barriers as shown in Fig. 1(a). We describe the potential of each barrier by a realistic model of the form

$$V_b(x)=V_0\cos^{2\beta}(\pi x/b)\ ,\quad -b/2\le x\le b/2\ , \tag{31}$$

where b is the width of the barrier, V_0 and integral β control the strength and steepness of the modulation, respectively. In the present calculations, we choose $\beta=1$ [see Fig. 1(b) for the potential $V_b(x)$ in the barrier regions in this case]. The barriers are separated by a distance $c=a-b$ and the potential in the regions between the barriers is simply set to zero. Here, we note that our model potential is continuous in the direction of the current flow, and so is its first-order derivative. The detailed shape of the confining potential [i.e., $V_c(y)$ in Eq. (1)] across the Q1D channel is not important in the present study. We, therefore, define the channel by the hard-wall confinement for simplicity. All our calculations presented in the following have been performed with the assumption of an effective mass $m^*=0.067m_e$, which is appropriate to the $Al_xGa_{1-x}As/GaAs$ interface.

We begin with the study of the conductance at a fixed magnetic field B as a function of w (the width of the Q1D channel). Figure 2 shows the calculated results for the channel with $M=20$ and five modulation strengths V_0 when no magnetic field is applied ($B=0$ T). The calculations have been done for two Fermi energies. Figure 2(a) shows the calculations for $E_F=10$ meV, while Fig. 2(b) shows that for $E_F=14$ meV. The electron transmission is not possible at these Fermi energies for $w<20$ nm. The confining potential of the channel gives rise to a set of electron subbands with sublevel energies E_n as their band edges. At $B=0$ T, $E_n=(\hbar^2/2m^*)(n\pi/w)^2$ and is lowered as w increases. The electron transmission through subband n can take place only when $E_n<E_F$. However, because of the periodic modulation, the subband will split into minibands separated by minigaps. The electron transmission is blocked when the Fermi energy is in a minigap. This is seen as the appearance of a dip in the calculated conductance as shown in Fig. 2. The formation of minigaps is observable even when the modulation is as weak as $V_0=0.2$ meV. For example, two sharp dips followed by a shallow dip are clearly seen in each conductance plateau of the channel at $V_0=0.2$ meV [see the lowest curve in Figs. 2(a) and 2(b)]. The channel widths at which the minigaps and, thus, the conductance dips appear can be estimated for each subband by using the Bragg reflection condition $k_n=m\pi/a$, where n is the index of the subband and m is the index of minigaps in the subband. Using $k_n=[(2m^*E_F/\hbar^2)-(n\pi/w)^2]^{1/2}$, one may find that the separation (in terms of the channel width w) between the two sharp dips at the edge of a conductance plateau increases approximately linearly with the subband index n. This is in agreement with our exact numerical calculations as shown in Fig. 2.

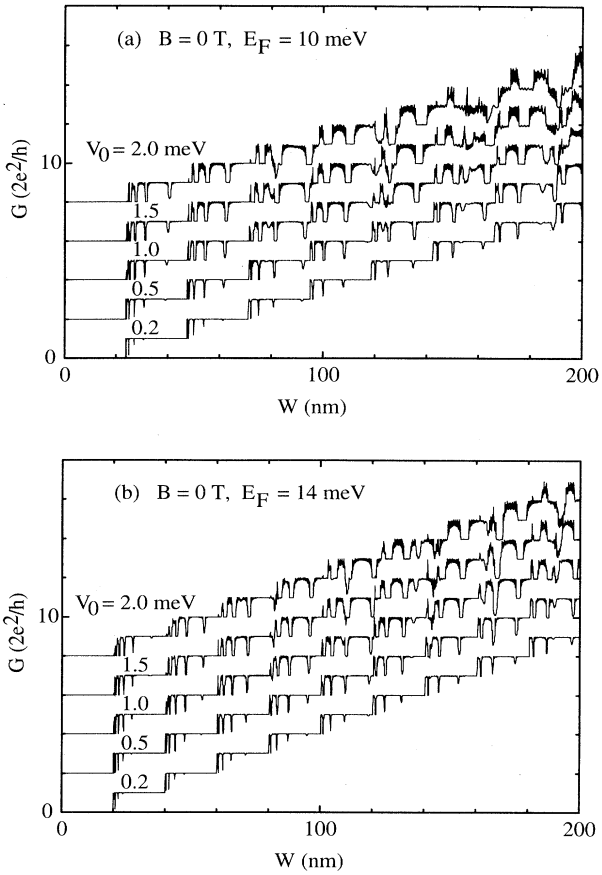

FIG. 2. Conductance G vs the channel width w at the zero magnetic field for the lateral surface superlattice shown in Fig. 1 with five modulation strengths V_0 and the following parameters: $\beta=1$, $a=150$ nm, $b=50$ nm, $c=100$ nm, $L_T=x_0^R-x_0^L=2960$ nm, and $M=20$. (a) shows the calculations for $E_F=10$ meV. (b) shows that for $E_F=14$ meV.

Figure 2 shows also that as the modulation strength V_0 increases, no significant change in the positions of the conductance dips is observed, but the dips are seen to widen up toward large width value. At strong modulation, minigaps (as well as minibands) that develop from different subbands may overlap, leading to some irregular structure in the conductance spectra. For example, at $V_0=2.0$ meV and $E_F=10$ meV [Fig. 2(a)] some dips and peaks are seen to appear irregularly in conductance plateaus with index $n\ge 3$. Such an irregular structure can also be seen in the calculations for $V_0=2.0$ meV and $E_F=14$ meV [Fig. 2(b)] and the calculations for some relatively weak modulations at both Fermi energies. The rapid oscillations are also seen in Fig. 2 in the cases of strong modulations. These oscillations originate from the coupling of the quasi-zero-dimensional (Q0D) states in the cavities formed between the modulation barriers. However, the number of oscillations between two adjacent conductance dips, in general, has no direct

correspondence to the number of cavity regions. This is again due to the presence of overlaps between the minibands and that between the minigaps.

When a magnetic field is applied perpendicularly to the modulated Q1D channel, electrons tend to move along the edges of the channel and the change in the characteristic of the calculated conductance is, therefore, expected. Figure 3 shows the results of our calculations at $B=1$ and 2 T. Two modulation strengths are considered in the calculations. The calculations for a relatively weak modulation ($V_0=0.5$ meV) are shown in Figs. 3(a) and 3(c), while the calculations for a strong modulation ($V_0=3.0$ meV) are shown in Figs. 3(b) and 3(d). It is seen that at the considered Fermi energies ($E_F=10$ and 14 meV), the applied magnetic field ($B=1$ and 2 T) has little effect on the calculated conductance when the width of the channel $w<40$ nm. This can be easily understood, because in this case, only the lowest subband of the quantum channel is open for electron transmission and the free cyclotron energy $\hbar\omega_c$ is much less than the energies of the subband. Therefore, the feature of the edge state transport is not significant. But this feature should emerge as the width of the Q1D channel increases and becomes much larger than the magnetic length l_B ($l_B=25.66$ nm at $B=1$ T and 18.14 nm at $B=2$ T).

Figures 3(a) and 3(c) show that for the weak modulation at $V_0=0.5$ meV, the regular minigap structure as observed at $B=0$ T is no longer seen at the calculated conductance at $B=1$ and 2 T, when w gets approximately larger than 80 nm. This may be interpreted as follows. In terms of the Bragg reflections, the formation of minigaps can be attributed to the formation of standing waves, due to wave interference between the forward and backward propagating electron states at the Fermi energy E_F. At $B=0$ T, the forward and backward states locate in the same region across the channel, giving a maximum probability for wave interference between them. When the magnetic field is applied, the forward and backward states tend to separate in their locations, leading to a diminution in the probability for their interference and thus the formation of minigaps. However, for a channel which is not very wide, the backscattering as a result of coupling between the forward and backward states can still take place at a relatively low magnetic field, due to the presence of the potential modulation. Therefore, we shall still see many dips in the calculated conductance for

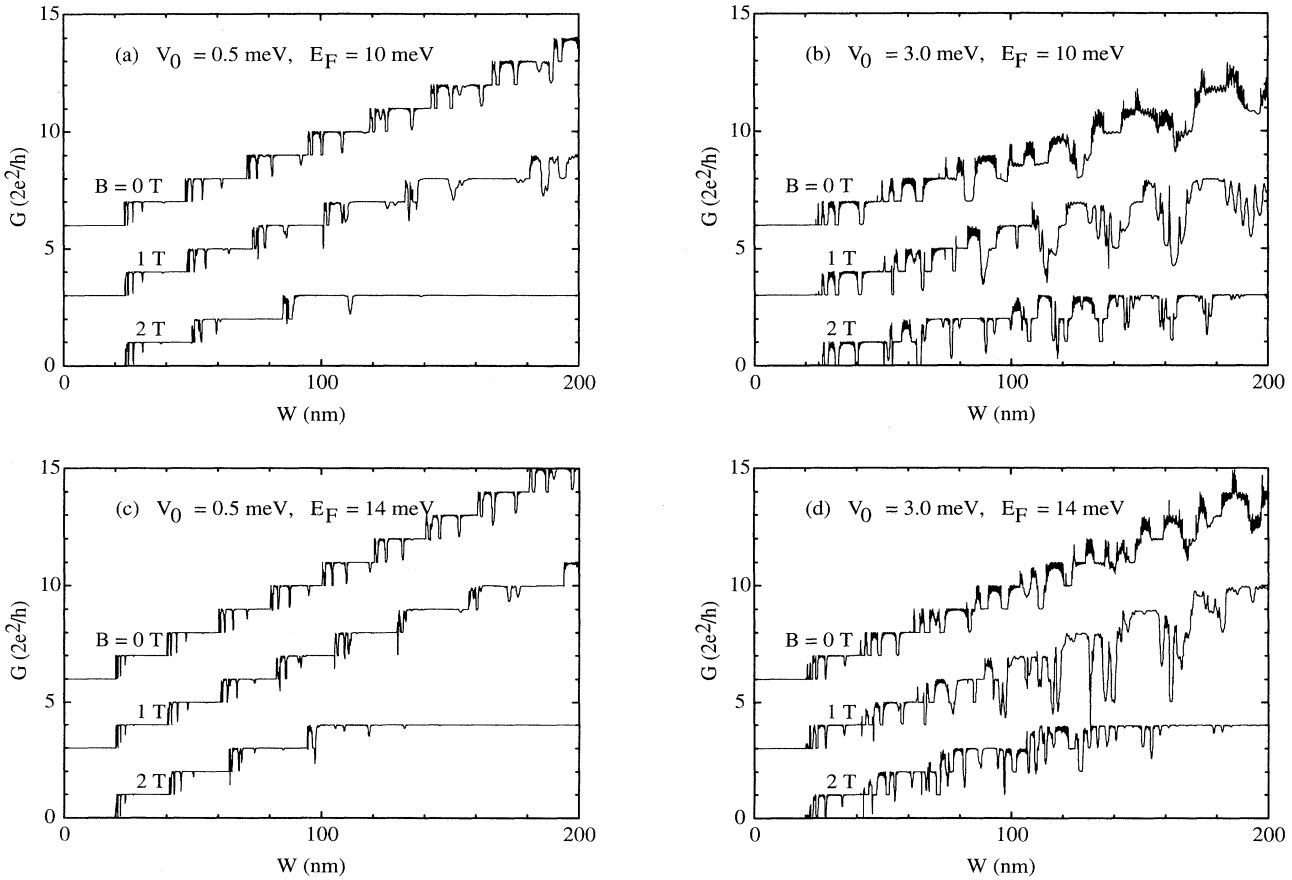

FIG. 3. Conductance G vs the channel width w at $B=0$, 1, and 2 T for the lateral surface superlattice shown in Fig. 1 with the parameters: $\beta=1$, $a=150$ nm, $b=50$ nm, $c=100$ nm, $L_T=x_0^R-x_0^L=2960$ nm, and $M=20$. The modulation strength and the Fermi energy assumed in the calculations are (a) $V_0=0.5$ meV and $E_F=10$ meV, (b) $V_0=3.0$ meV and $E_F=10$ meV, (c) $V_0=0.5$ meV and $E_F=14$ meV, and (d) $V_0=3.0$ meV and $E_F=14$ meV.

$w > 80$ nm, as shown in Figs. 3(a) and 3(c), although their appearances become irregular now. When $w \gg l_B$, this kind of back scattering is expected to be suppressed and, as we see in Figs. 3(a) and 3(c) for the calculations at $B = 2$ T and $w > 100$ nm, the conductance vs w should become structureless.

The suppression of miniband-associated conductance dips by applied magnetic field are also seen in the calculations for the quantum channel with the relatively strong modulation of $V_0 = 3$ meV, as shown in Figs. 3(b) and 3(d). Again, the irregular conductance structure seen in calculations for $B = 0$ T and $w > 100$ nm [Figs. 3(b) and 3(d)] originates from the overlaps between the minibands and that between the minigaps formed from different subbands, while the rapid oscillations reflect electron transmission through coupled Q0D states in the modulated channel and should form continuous conductance plateaus when the number of potential barriers M goes to infinity. At $B \neq 0$ T, particularly in the case of $B = 2$ T and $E_F = 14$ meV, many minigap-associated conductance dips are seen to be replaced by the dips originating from the back scattering via the electron states propagating along the two edges of the channel. Because of the strong modulation, the latter are very pronounced over a much wider range of value w compared with the calculations for the weak modulation of $V_0 = 0.5$ meV [Figs. 3(a) and 3(c)].

Another interesting effect of magnetic field as seen in Figs. 3(b) and 3(d) is the suppression of the rapid conductance oscillations, i.e., the electron transmissions through coupled Q0D states. This can be understood as follows. It was shown that the Q0D states are most likely localized deep inside the channel.[35] However, the electron states at magnetic field tend to propagate along the edges of the channel. When the width of the channel becomes large enough, the propagating edge states can be decoupled from the Q0D state and the 1D characteristic of electron transport (i.e., the quantized conductance) will then be recovered. This recovery may clearly be recognized in the calculations for $B = 2$ T, as shown in the lowest curves of Figs. 3(b) and 3(d). We recall that the dips seen in the recovered quantized plateaus are due to the backscattering via the coupling between the electron states propagating along the opposite edges of the channel. This coupling should mostly take place in the barrier regions.

Finally, we show in Fig. 4 the results of our calculations for the conductance as a function of the Fermi ener-

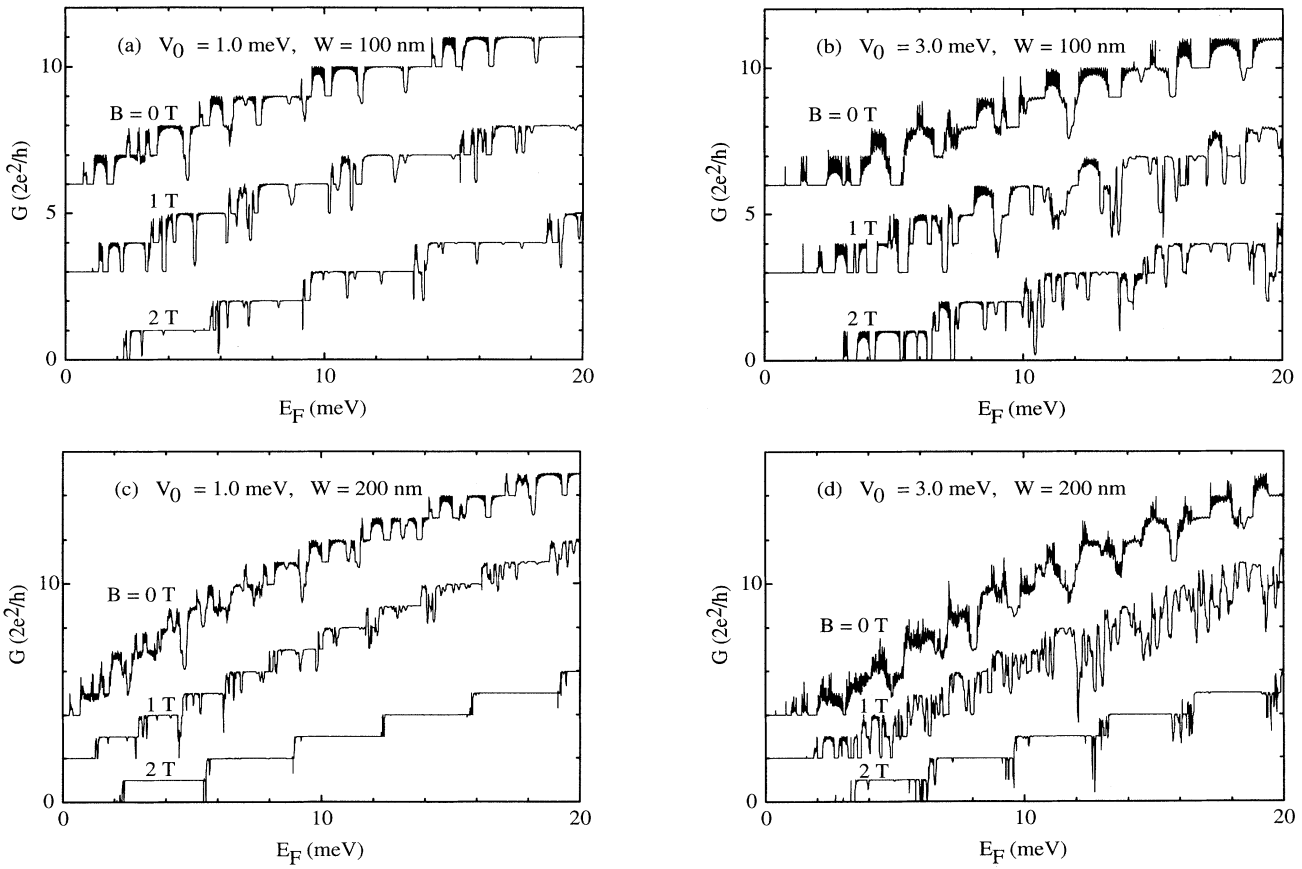

FIG. 4. Conductance G vs the Fermi energy E_F at $B = 0$, 1, and 2 T for the lateral surface superlattice shown in Fig. 1 with the parameters: $\beta = 1$, $a = 150$ nm, $b = 50$ nm, $c = 100$ nm, $L_T = x_0^R - x_0^L = 2960$ nm, and $M = 20$. The modulation strength and the channel width assumed in the calculations are (a) $V_0 = 1.0$ meV and $w = 100$ nm, (b) $V_0 = 3.0$ meV and $w = 100$ nm, (c) $V_0 = 1.0$ meV and $w = 200$ nm, and (d) $V_0 = 3.0$ meV and $w = 200$ nm.

gy E_F when the width of quantum channel is fixed. Figures 4(a) and 4(b) [Figs. 4(c) and 4(d)] show our calculations for $w=100$ nm ($w=200$ nm), but $V_0=1.0$ and 3.0 meV, respectively. At $B=0$ T, we again see conductance dips associated with the formation of minigaps and rapid oscillations reflecting the electron transmission through the coupled Q0D states in the cavity regions between the barriers. Both are suppressed or partly at $B=1$ and 2 T. Many new dips seen in the calculations at $B=1$ and 2 T for $w=100$ nm [Figs. 4(a) and 4(b)] and in the calculations at $B=1$ T for $w=200$ nm [Figs. 4(c) and 4(d)] again originate from the backscattering via the coupling between the electron states propagating along the opposite edges of the channel. It is interesting to note that due to the presence of a large number of such new dips, the calculated conductance at $B=1$ T for $V_0=3.0$ meV and $w=200$ nm [Fig. 4(d)] are actually seen to display fluctuations. These fluctuations are rather slow compared with the oscillations seen in the calculated conductance at $B=0$ T.

In addition, we see in Figs. 4(c) and 4(d) a rather perfect recovery of the conductance quantization at $B=2$ T and $w=200$ nm, although sharp resonant structure may still be seen at the edge of each plateau. This is in agreement with our results presented in Fig. 3, where a large suppression of backscattering of the propagating edge states at $B=2$ T and w close to 200 nm can be seen. The sharp resonant structure seen particularly in the lowest curve of Fig. 4(d) indicates that at high magnetic field the backscattering can take place only when the Fermi energy E_F lies in the neighborhood of a magnetoelectric-subband edge of the Q1D channel.

IV. SUMMARY AND CONCLUDING REMARKS

We have presented a method for the calculations of electron transport through lateral quantum systems in a magnetic field, based on scattering-matrix formalism. The transfer matrices needed in the implementation of the method are derived and some features that appear as a result of the presence of the magnetic field are discussed. Since its formulation has been developed by representing all required matrices in a common basis, the method has a great flexibility, i.e., it can easily be used to treat electron transport through a quantum system modulated with a complicated potential profile.

As an example of its application, the method has been used to investigate the effects of an applied magnetic field B on electron transport through a periodically modulated Q1D channel. We have modeled the modulation potential by a realistic, smooth function and have calculated the conductance of the system as a function of the channel width w and as a function of the Fermi energy E_F. The results of these calculations are presented in Figs. 2–4.

At $B=0$ T, in addition to the well-known quantized conductance plateaus, the calculated conductance vs the channel width w displays regular dips. We have found that the values of w at which the dips appear do not change significantly as the modulation strength V_0 increases. However, at strong modulation the dips are found to widen up towards wide width w and the rapid oscillations are seen to appear between the dips. The conductance structure of the system can, therefore, be complicated in this case. We have interpreted the dips as a result of the formation of minigaps (or the Bragg reflections) and the rapid oscillations as electron transmission through the coupled Q0D states in the cavity regions between the potential barriers.

When a magnetic field is applied perpendicularly to the Q1D channel, the suppressions of both the minigap-associated conductance dips and the rapid oscillations are seen in the calculated conductance vs the channel width w. This is because the electron states propagating in the opposite directions tend to locate along the opposite edges of the channel, leading to the reductions in the probabilities for the Bragg reflections and for the coupling between the propagating edge states and the Q0D states located deep inside the channel. However, the conductance dips may appear irregularly in the system. These dips reflect the existence of the backscattering via the coupling between the electron states propagating along the opposite edges of the channel as a result of the presence of the potential barriers. When the channel width w becomes much larger than the magnetic length l_B, these irregular dips are seen to be also suppressed by the applied magnetic field. The calculations for the conductance vs the Fermi energy E_F show rather similar results. However, the features of the propagating-edge-state transport are more clearly displayed in these calculations. It has been shown that in the presence of a magnetic field, the dips due to the backscattering of the propagating edge states can appear in a wide channel with a relatively strong modulation so densely that the conductance actually exhibits fluctuations. It has also been shown that these fluctuations can be washed out in the high-field regime, leading to a nearly perfect recovery of the conductance quantization.

ACKNOWLEDGMENTS

The author is grateful to K.-F. Berggren, P. Omling, and L. Samuelson for many helpful suggestions and discussions. This work, which is performed within the Nanometer Structure Consortium in Lund, has been supported by the Swedish Natural Science Research Council and the Swedish National Board for Industrial and Technical Development.

APPENDIX

In the presence of a perpendicular magnetic field, the electric current $J(E_F,k_{I\gamma})$ carried through a lateral quantum channel by an electron state $\Psi(x,y)$ associated with the incident wave $e^{ik_{I\gamma}(x-x_0^L)}\varphi_{I\gamma}(y)$ from left at energy E_F is given by

$$J(E_F,k_{I\gamma})=-\frac{e}{2}\int_{-w/2}^{w/2}dy[\Psi^*(x,y)\hat{v}_x\Psi(x,y) +\Psi(x,y)\hat{v}_x^*\Psi^*(x,y)]\ , \quad \text{(A1)}$$

where the electron charge, $-e$, has been assumed and

$\hat{v}_x$ is the electron velocity operator in the magnetic field,

$$\hat{v}_x=\frac{1}{m^*}\left[-i\hbar\frac{\partial}{\partial x}-eBy\right] . \tag{A2}$$

Inserting Eq. (15) into Eq. (A1), the current $J(E_F,k_{I\gamma})$ can be rewritten, in terms of the eigensolutions $\{k^i_{I\alpha},\varphi^i_{I\alpha}(y)\}$ and $\{k^i_{II\alpha},\varphi^i_{II\alpha}(y)\}$ in one of the narrowly divided strip regions or in one of the two leads, as

$$\begin{aligned}J(E_F,k_{I\gamma})=-e\sum_\alpha\sum_\beta\Bigg\{&a^*_{I\alpha}a_{I\beta}e^{-i(k^*_{I\alpha}-k_{I\beta})(x-x_0)}\frac{\hbar}{2m^*}\int_{-w/2}^{w/2}dy\left[k^*_{I\alpha}+k_{I\beta}-\frac{2y}{l_B^2}\right]\varphi^*_{I\alpha}(y)\varphi_{I\beta}(y)\\&+a^*_{II\alpha}a_{II\beta}e^{-i(k^*_{II\alpha}-k_{II\beta})(x-x_0)}\frac{\hbar}{2m^*}\int_{-w/2}^{w/2}dy\left[k^*_{II\alpha}+k_{II\beta}-\frac{2y}{l_B^2}\right]\varphi^*_{II\alpha}(y)\varphi_{II\beta}(y)\\&+a^*_{I\alpha}a_{II\beta}e^{-i(k^*_{I\alpha}-k_{II\beta})(x-x_0)}\frac{\hbar}{2m^*}\int_{-w/2}^{w/2}dy\left[k^*_{I\alpha}+k_{II\beta}-\frac{2y}{l_B^2}\right]\varphi^*_{I\alpha}(y)\varphi_{II\beta}(y)\\&+a^*_{II\alpha}a_{I\beta}e^{-i(k^*_{II\alpha}-k_{I\beta})(x-x_0)}\frac{\hbar}{2m^*}\int_{-w/2}^{w/2}dy\left[k^*_{II\alpha}+k_{I\beta}-\frac{2y}{l_B^2}\right]\varphi^*_{II\alpha}(y)\varphi_{I\beta}(y)\Bigg\} .\end{aligned} \tag{A3}$$

Here, the region index (i, L, or R) has been dropped. Using Eq. (6), we see immediately that the first and second terms in the braces can be nonzero only if $\alpha=\beta$ and the eigenwave numbers $k_{I\alpha}=k_{I\beta}$ and $k_{II\alpha}=k_{II\beta}$ are purely real. However, for the last two terms in the braces to be nonzero, the eigenwave numbers $k_{i\alpha},k_{I\beta},k_{II\alpha}$, and $k_{II\beta}$ have to be imaginary or complex with a nonzero imaginary part. Furthermore, if the eigensolutions $\{k^i_{I\alpha},\varphi^i_{I\alpha}(y)\}$ and $\{k^i_{II\alpha},\varphi^i_{II\alpha}(y)\}$ are numbered in such a way that $k^*_{I\alpha}=k_{II\alpha}$ and $\varphi^*_{I\alpha}(y)=\varphi_{II\alpha}(y)$ for both imaginary and complex $k_{I\alpha}$ and $k_{II\alpha}$,[36] one of the required conditions for the last two terms in the braces to be nonzero is again $\alpha=\beta$. Having all these in mind, we can now write Eq. (A3) in a compact form,

$$\begin{aligned}J(E_F,k_{I\gamma})=-e\Bigg[&\sum_\alpha^{(R)}(v_{I\alpha}|a_{I\alpha}|^2+v_{II\alpha}|a_{II\alpha}|^2)\\&+\sum_\alpha^{(C)}(v_{II\alpha}a^*_{I\alpha}a_{II\alpha}+v_{I\alpha}a_{I\alpha}a^*_{II\alpha})\Bigg] ,\end{aligned} \tag{A4}$$

where (R) indicates that the sum is taken over those values of α for which $k_{I\alpha}$ and $k_{II\alpha}$ (thus $v_{I\alpha}$ and $v_{II\alpha}$) are real, while (C) indicates that the sum is taken over those values of α for which $k_{I\alpha}$ and $k_{II\alpha}$ (thus $v_{I\alpha}$ and $v_{II\alpha}$) are either imaginary or complex. A further simplification of the equation can be achieved if the current is evaluated in a lead. In the left lead, $a^L_{I\alpha}=\delta_{\alpha\gamma}$ and both $v_{I\alpha}$ and $v_{II\alpha}$ are real when $\alpha=\gamma$. The current is then

$$J(E_F,k_{I\gamma})=-e\left[v^L_{I\gamma}+\sum_\alpha^{(R)}v^L_{II\alpha}|a^L_{II\alpha}|^2\right] . \tag{A5}$$

In the right lead, $a^R_{II\alpha}=0$ for all α's. The current is thus

$$J(E_F,k_{I\gamma})=-e\sum_\alpha^{(R)}v^R_{I\alpha}|a^R_{I\alpha}|^2 . \tag{A6}$$

Combining Eqs. (A5) and (A6) gives the familiar relationship,

$$\sum_\alpha^{(R)}(T_{\gamma\alpha}+R_{\gamma\alpha})\equiv\sum_\alpha^{(R)}\left[\frac{v^R_{I\alpha}}{v^L_{I\gamma}}|a^R_{I\alpha}|^2-\frac{v^L_{II_\alpha}}{v^L_{I\gamma}}|a^L_{II\alpha}|^2\right]=1 , \tag{A7}$$

where $T_{\gamma\alpha}=(v^R_{I\alpha}/v^L_{I\gamma})|a^R_{I\alpha}|^2$ and $R_{\gamma\alpha}=-(v^L_{II\alpha}/v^L_{I\gamma})|a^L_{II\alpha}|^2$ are known as the transmission and the reflection coefficients, respectively.

[1]D. K. Ferry and R. O. Grondin, *Physics of Submicron Devices* (Plenum, New York, 1991).

[2]*Physics of Nanostructures*, Proceedings of the 38th Scottish Universities Summer School in Physics, edited by J. H. Davies and A. R Long (Institute of Physics, Bristol, 1992).

[3]C. W. J. Beenakker and H. van Houten, in *Solid State Physics: Advances in Research and Applications*, edited by H. Ehrenreich and D. Turnbull (Academic, San Diego, 1991), Vol. 44, p. 1.

[4]B. J. van Wees, H. van Houten, C. W. J. Beenakker, J. G. Williamson, L. P. Kouwenhoven, D. van der Marel, and C. T. Foxon, Phys. Rev. Lett. **60**, 848 (1988).

[5]D. A. Wharam, T. J. Thornton, R. Newbury, M. Pepper, and H. Ahmed, J. Phys. C **21**, L209 (1988).

[6]N. K. Patel, L. Martin-Moreno, M. Pepper, R. Newbury, J. E. F. Frost, D. A. Ritchie, G. A. C. Jones, J. T. M. B. Janssen, J. Singleton, and J. A. A. J. Perenboom, J. Phys. Condens. Matter **2**, 7247 (1990).

[7]N. K. Patel, J. T. Nicholls, L. Martin-Moreno, M. Pepper, J. E. F. Frost, D. A. Ritchie, and G. A. Jones, Phys. Rev. B **44**, 13 549 (1991).

[8]A. Szafer and A. D. Stone, Phys. Rev. Lett. **62**, 300 (1989).

[9]E. G. Haanappel and D. van des Marel, Phys. Rev. B **39**, 5484 (1989).
[10]G. Kirczenow, Solid State Commun. **68**, 715 (1988); J. Phys. Condens. Matter **1**, 305 (1989); Phys. Rev. B **39**, 10 452 (1989).
[11]E. Tekman and S. Ciraci, Phys. Rev. B **39**, 8772 (1989); **40**, 8559 (1989).
[12]L. Escapa and N. Garcia, J. Phys. Condens. Matter **1**, 2125 (1989).
[13]M. Büttiker, Phys. Rev. B **41**, 7906 (1990).
[14]L. I. Glazman and A. V. Khaetskii, Europhys. Lett. **9**, 263 (1989).
[15]L. Martin-Moreno, J. T. Nicholls, N. K. Patel, and M. Pepper, J. Phys. Condens. Matter **4**, 1323 (1992).
[16]Hongqi Xu, Phys. Rev. B **47**, 15 630 (1993).
[17]L. P. Kouwenhoven, F. W. J. Hekking, B. J. van Wees, C. J. P. M. Harmans, C. E. Timmering, and C. T. Foxon, Phys. Rev. Lett. **65**, 361 (1990).
[18]S. E. Ulloa, E. Castaño, and G. Kirczenow, Phys. Rev. B **41**, 12 350 (1990).
[19]J. A. Brum, Phys. Rev. B **43**, 12 082 (1991).
[20]Hua Wu, D. W. L. Sprung, J. Martorell, and S. Klarsfeld, Phys. Rev. B **44**, 6351 (1991).
[21]Hua Wu and D. W. L. Sprung, Phys. Rev. B **47**, 1500 (1993).
[22]Hongqi Xu, Zhen-Li Ji, and K.-F. Berggren, Superlatt. Microstruct. **12**, 237 (1992).
[23]Hongqi Xu, Phys. Rev. B **47**, 9537 (1993).
[24]E. N. Economou and C. M. Soukoulis, Phys. Rev. Lett. **46**, 618 (1981); D. S. Fisher and P. A. Lee, Phys. Rev. B **23**, 6851 (1981); P. A. Lee and D. S. Fisher, Phys. Rev. Lett. **47**, 882 (1981); L. Schweizer, B. Kramer, and A. MacKinnon, J. Phys. C **17**, 4111 (1984); Z. Phys. B **59**, 379 (1985); A. MacKinnon, *ibid.* **59**, 385 (1985).
[25]M. Leng and C. S. Lent, Phys. Rev. Lett. **71**, 137 (1993); Phys. Rev. B **50**, 10 823 (1994).
[26]Hongqi Xu, Phys. Rev. B **50**, 8469 (1994).
[27]In fact, x^i can be chosen to be any x value within the ith narrow strip and the calculation for electron transport should be insensitive to its choice when the number of strips divided in the modulated channel N is very large so that all the strips are extremely narrow. In the actual calculations, we let N increase until our required accuracy is achieved.
[28]J. Kucera and P. Streda, J. Phys. C **21**, 4357 (1988).
[29]R. L. Schult, H. W. Wyld, and D. G. Ravenhall, Phys. Rev. B **41**, 12 760 (1990).
[30]H. Tamura and T. Ando, Phys. Rev. B **44**, 1792 (1991).
[31]D. Y. K. Ko and J. C. Inkson, Phys. Rev. B **38**, 9945 (1988).
[32]M. Büttiker, Phys. Rev. Lett. **57**, 1761 (1986).
[33]P. Streda, J. Kucera, and A. H. MacDonald, Phys. Rev. Lett. **59**, 1973 (1987).
[34]J. K. Jain and S. A. Kivelson, Phys. Rev. B **37**, 4276 (1988).
[35]Zhen-Li Ji, Phys. Rev. B **50**, 4658 (1994).
[36]This numbering is possible, because if k_α and $\varphi_\alpha(y)$ (we have omitted the subbasis labels *I* and *II*) are a solution of Eq. (4), their complex conjugates k_α^* and $\varphi_\alpha^*(y)$ are also a solution.